

# Assessing the effects of date and sequence data in phylodynamics

Leo A. Featherstone<sup>\*,1</sup>, Sebastian Duchene<sup>1</sup>, Timothy G. Vaughan<sup>2,3</sup>

<sup>1</sup> Peter Doherty Institute for Infection and Immunity, University of Melbourne, Australia.

<sup>2</sup> Department of Biosystems Science and Engineering, ETH Zurich, Basel, Switzerland.

<sup>3</sup> Swiss Institute of Bioinformatics.

email: leo.featherstone@unimelb.edu.au

## Abstract

Birth-death based methods are often used to infer epidemiological parameters from pathogen genomes in phylodynamics. However, these methods also base their results on sampling time data in addition to genome sequence data. We introduce a formal method for quantifying the relative impacts of the date and sequence components of the data. We show that either data source can drive inference of the basic reproductive number,  $R_0$ , but note that the general approach can be used to investigate other phylodynamic parameters. This framework will allow practitioners to draw conclusions about which aspect of the data drive inference results, providing a path to a deeper understanding of commonly-used phylodynamic models and to better direct sequencing efforts during future outbreaks.

## Introduction

Phylodynamics combines phylogenetic and epidemiological modelling to infer epidemiological dynamics from pathogen genome data (du Plessis and Stadler, 2015; Baele et al., 2018; Volz et al., 2013). Analyses are usually conducted within a Bayesian framework, meaning that the output comprises posterior distributions for parameters of interest, such as the basic reproductive number,  $R_0$  (i.e. the average number of secondary infections in a fully susceptible population). Input data usually

consists of time-stamped genome sequences. In the case of birth-death-sampling models (Stadler, 2010), both sequence and date data inform the branching of inferred trees by either temporally clustering lineages or via sequence similarity. Internal nodes are assumed to co-occur with transmission events, such that they provide information about patterns of transmission that sampling time data alone cannot. Sampling times, or date data, are similar to standard epidemiological time series data while sequence data introduce the evolutionary aspect. The widely used birth-death model uses sampling times to infer a sampling rate which is also informative about transmission rates (Boskova et al., 2018; Stadler et al., 2012).

Phylogenetics is experiencing greater use than ever before since the onset of the SARS-CoV-2 pandemic. This commonly includes application to larger and more densely sequenced outbreaks than previously. While the value of pathogen genome data is now well established, an emergent question is whether inclusion of more sequence data after a point is of diminishing returns for some densely sequenced outbreaks. The answer to this question will naturally vary with each dataset and pathogen considered, but a method to quantify the individual effects of date and sequence data presents a transferable way to address it. It would substantially broaden our understanding of the phylogenetic tools that now feature in infectious disease surveillance. It also has the potential to direct sampling efforts to future outbreaks for optimisation of knowledge gain against resource expenditure.

Earlier work showed that sequence sampling times, referred to here as 'date data', can drive epidemiological inference under the birth-death model (Volz and Frost, 2014; Boskova et al., 2018; Featherstone et al., 2021). However, each stopped short of proposing a transferable way to measure this effect in regular application. The birth-death model is most applicable to the question at hand since it includes a rate of sampling. The coalescent is another a key phylogenetic model, but it typically conditions on sampling dates which therefore precludes from a comparison of date and sequence effects. Some coalescent formulations include a sampling rate (Volz and Frost, 2014), however these are used less often than the birth death or standard coalescent. The coalescent also assumes a low sampling proportion relative to population size such that its typical formulation would

52 be inappropriate for many densely sequenced outbreaks (Boskova et al., 2018), where the question  
 53 of the effect of large amounts of sequence data is most relevant.

54 Building upon these earlier results, we introduce a theoretical framework and a new method to  
 55 quantify the effect of sequence and dates for any parameter under the birth death with continuous  
 56 sampling. We focus on continuous sampling because it is most relevant to how emerging outbreak  
 57 data are collected. Our method quantifies and visualises the effect each data source has on the  
 58 posterior distribution of epidemiological parameters of interest. It also classifies which data source  
 59 is driving the inference, but crucially also provides a measure of whether a binary classification  
 60 is meaningful. These observations are a critical addition the phylodynamic toolkit used to inform  
 61 public health decisions because they clearly quantify the added-knowledge acquired from genomes  
 62 in a given analysis.

Table 1: Separating data to quantify effects

	Dates Included	Dates Excluded
Sequence Included	Combined effect	Sequence Effects
Sequence Excluded	Date effects	Marginal Prior

## New Methods

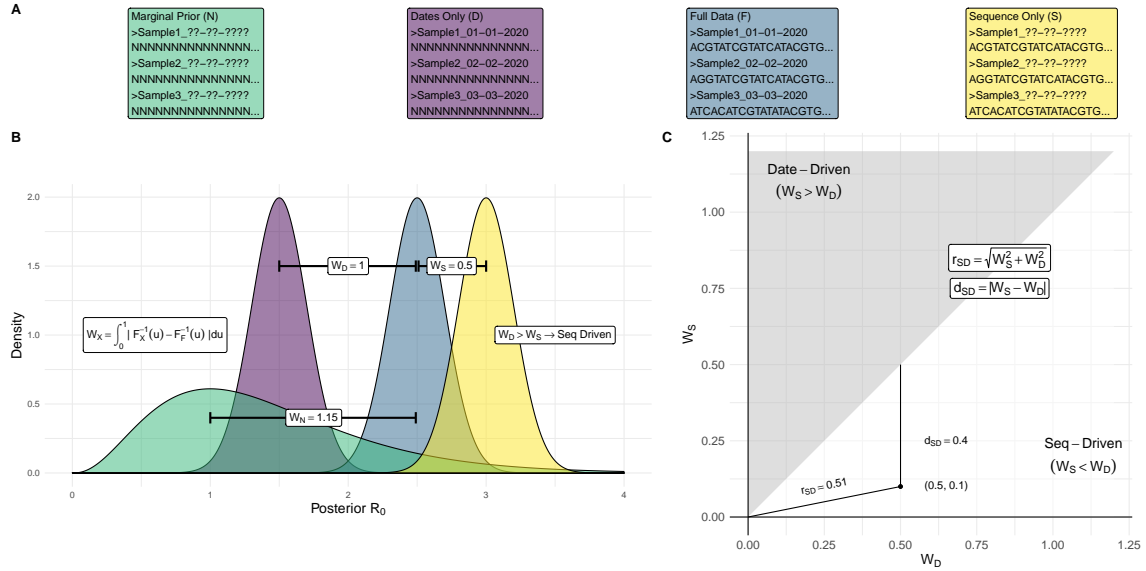


Figure 1: Graphical summary of the process to quantify signal and classify signal drivers. **A)** Coloured boxes give examples of data under each of the 4 treatments with letters in brackets giving shorthand notation for each. From left to right: *Marginal Prior* results from the removal of both date and sequence data. *Dates Only* includes date data while ignoring sequence data through a constant phylogenetic likelihood. This can be represented as converting all sequence characters to ‘N’ (i.e. alignments of fully missing data). *Full data* represents the usual combination of both sequence and date data. This produces a reference distribution from which the Wasserstein metric to other posteriors is calculated. *Sequence Only* corresponds to the removal and re-estimation of dates while sequence data is retained. **B)** Example posterior output for  $R_0$  with colour corresponding to each treatment in **A**. The Wasserstein metric is calculated as difference in inverse distribution function of each posterior from *Full Data* integrated over 0 to 1. Example values for the Wasserstein metric are given in white boxes. **C)** The plane with x and y axes  $W_D$  and  $W_S$  and shaded classification regions.  $r_{SD}$  is the Euclidean distance from the origin to a point  $(W_D, W_S)$ , with higher values indicating that one or both of data and sequence data drive differing signals from the reference posterior.  $d_{SD}$  is the vertical distance from a point  $(W_D, W_S)$  to the line  $y = x$ , with points closer to this line corresponding to more similar data and sequence data effects such that classification is less meaningful. In the example, distance from the posterior under only sequence data to the full data posterior ( $W_S$ ) is smallest, leading to classification as ‘Seq-Driven’.

## Isolating date and sequence data

We conduct four analyses for a given dataset to contrast the effects of complete data, date data, sequence data, and the absence of both (fig 1A). We focus on inferring  $R_0$ , with all other parameters fixed, but this new approach is applicable to any parameter under the birth-death with any combination of priors. First, we use complete data to fit a birth-death model and infer the posterior distribution of  $R_0$ . This represents the combined effects of dates and sequences. Second, to isolate

the effect of date data, we remove sequence information and retain dates, thus integrating over the prior on tree topology. This is traditionally referred to as 'sampling from the prior', but this term should be avoided in the context of models where the sampling times are treated as data, such as the birth-death. Third, to isolate the effect of sequence data, we keep sequence data and remove dates. This requires estimation of all sampling dates, analogously to how removing sequence data causes integration over topology. We use a novel Markov chain Monte Carlo (MCMC) operator to estimate dates which is implemented in the `feast v17` package for BEAST 2 (Bouckaert et al., 2019). Last, and for completeness, we conduct the analysis with both date and sequence data removed. This formally corresponds to the marginal prior conditioned on the number of samples. The resulting Wasserstein metric,  $W_N$ , is useful for quantifying whether full data offer information in addition to the prior.

## Quantifying data signal

We employ the Wasserstein metric in one dimension to measure a “distance” between each of the sequence posterior, date posterior, or marginal prior, and the posterior derived from the complete data. We write these distances as  $W_\bullet$ , with  $\bullet$  being  $D$ ,  $S$ , or  $N$  for the sequence, date, and marginal prior distributions, respectively. For example, the Wasserstein distance  $W_D$  from the date posterior to complete data as:

$$W_D = \int_0^1 |F_D^{-1}(u) - F_F^{-1}(u)| du,$$

where  $F_D^{-1}$  and  $F_F^{-1}$  are the inverse empirical distribution functions for the posterior  $R_0$  inferred under date and complete data respectively. The units of  $W_\bullet$  are equivalent to the units of the parameter of interest.

As in Fig 1C, we can now consider a plane where the axes are  $W_D$  and  $W_S$ . We classify the data source with the lowest Wasserstein distance from the complete data posterior as contributing most to the posterior with sequence and date data. In this case the lines  $y = x$  marks the classification boundary as in the shading in Fig 1C.

Finally, we can quantify the disagreement in signal between each data source. We define disagreement with respect to the full data posterior,  $r_{SD}$  as the magnitude of the vector  $(\overrightarrow{W_D, W_S})$  leading to each point in the plane, which is the radius from the origin to the point in other words. Values near zero indicate that the posteriors under data, sequence, and complete data are all near identical and classification of date or sequence driven is less meaningful. Larger values signify that one or both data sources drive differing posteriors and classification is more meaningful. We also define disagreement without respect to full data  $d_{SD} = |W_S - W_D|$  as a quantification of disagreement between date and sequence posteriors without respect to full data (Fig S1C). Visually, this corresponds to the vertical distance to the nearest classification boundary ( $y = x$ ) such that smaller values correspond to less meaningful classification.  $r_{SD}$  and  $d_{SD}$  are similar in that when  $r_{SD}$  is near-zero,  $d_{SD}$  necessarily is too.  $d_{SD}$  also accounts for the case where  $r_{SD}$  is high, but both date and sequence data have similarly sized effects. In this case,  $r_{SD}$  is higher while  $d_{SD}$  is lower and classification of one or another as driving analysis is inaccurate. Tree 8 in Fig 2 presents an example of this.

## Results

We simulated 400 alignments to explore the differing signals in date and sequence data using the Wasserstein metric. These derive from 100 simulated outbreaks of 100 cases, sampled with proportion 1 or 0.5, and used to simulate sequences with an evolutionary rate of  $10^{-3}$  or  $10^{-5}$  (subs/site/time). Higher evolutionary rates imply that there are more site patterns and therefore more informative sequence data. We estimated  $R_0$  under each data treatment with all other parameters fixed using a birth-death tree prior. In all analyses, simulated data provided information in addition to the prior ( $W_N > \approx 0$ , Fig S2). Among the 400 datasets, we observe a mixture of cases where date and sequence data infer similar or dissimilar posterior  $R_0$ . This supports the core assumption that date and sequence data can have differing signals concealed in their combination (Fig 2). Classification using the Wasserstein metric results in a mix of date and sequence driven classifications, supporting that our proposed method is sensitive to differences between datasets (Fig 3 A-C). Most datasets

were classified as date-driven (334/400), which is consistent with earlier work showing that dates are highly influential under the birth-death Volz and Frost (2014).

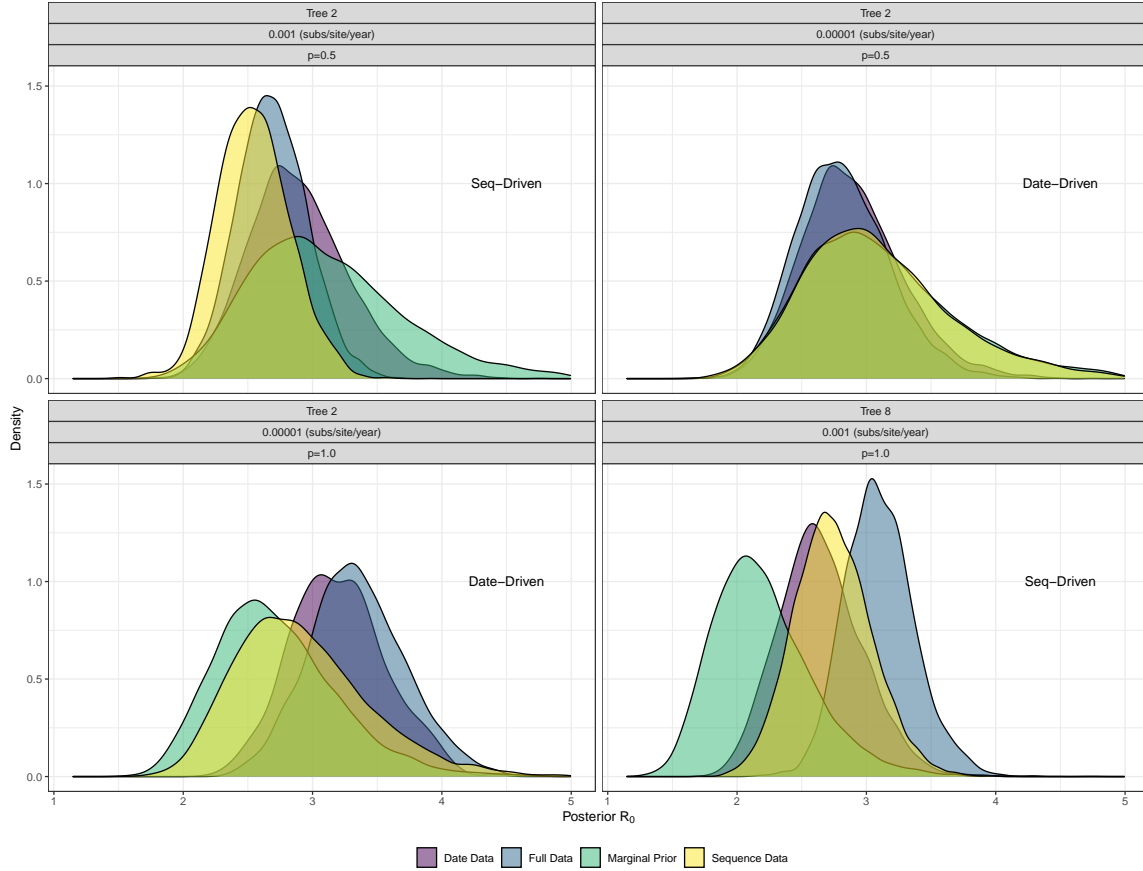


Figure 2: Comparison of full data, date data, sequence data, and no data posteriors for different trees and alignments. Each plot gives an example of posterior output for  $R_0$  under each treatment for different one of the 400 test datasets. Tree 8 gives an example of when both date and sequence posteriors are similar while differing from the full data posterior. Here,  $r_{SD}$  is higher, while  $d_{SD}$  is lower such that classification using the Wasserstein metric is both less meaningful and more likely to reflect noise due to MCMC sampling.

## Reliability of Wasserstein Metric

Alignments were simulated under two sampling conditions ( $p = 0.5$  and  $p = 1$ ) to test robustness with respect to sampling proportion. We found that sampling proportion does not bias the distribution of the Wasserstein statistic between analyses (Fig 3 D). This supports the assumption that comparing Wasserstein distance between analyses captures different signals concealed in date and sequence data.

123 We also tested the accuracy of classification using the Wasserstein metric by subsampling and  
124 reclassifying each posterior  $R_0$  distribution 100 times. Only 329 of resulting 40000 subsampled  
125 posteriors were misclassified across 17 of the 400 datasets (S1). Misclassification only occurred for  
126 datasets where  $d_{SD}$  was below  $10^{-1.47}$ . Smaller  $d_{SD}$  values indicate that the effect size of date and  
127 sequence data is similar and classification is not therefore not useful.



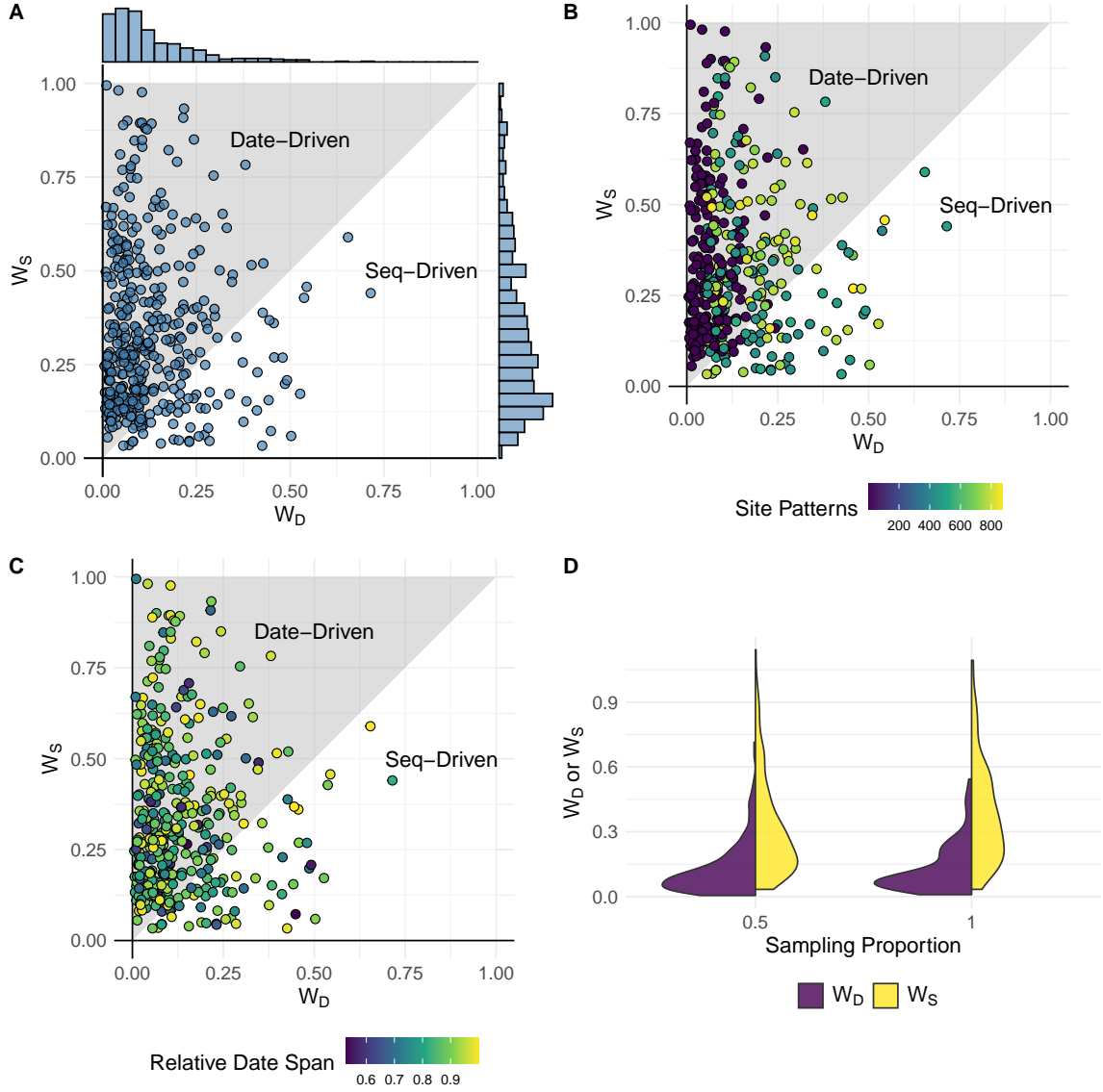


Figure 3: **A-C)** Each point represents  $(W_D, W_S)$  for one of the 400 simulated datasets. **A)** The distribution of points with marginal histograms corresponding to the distribution of  $W_D$  and  $W_S$  respectively. More datasets are classified as date-driven, which is consistent with prior results about the impact of sampling times under the birth-death. **B)** Points coloured by number of site patterns. Lower site patterns tends to co-occur with date-driven classification. **C)** Points coloured by date span with no clear patterns corresponding with classification as for site patterns. **D)** Distribution of  $W_S$  and  $W_D$  under  $p = 0.5$  and  $p = 1$ . The similarity of distributions across sampling proportion does not drive differences in  $W_S$  and  $W_D$ .

## Observations about the effects of Sequence and Dates

The distributions of  $W_S$  is more diffuse than  $W_D$ , meaning the sequence data posterior tends to differ more from full data than date data (Fig 3 A). This again aligns with previous results showing

131 that date data drive inference under the birth-death.

132 Low sequence diversity, measured here in the number of site patterns, seems to preclude sequence  
133 data from driving inference (Fig 3B, Fig S3). This matches the expectation that fewer site patterns  
134 results in less sequence information to inform the posterior. On the other hand, the date span does  
135 not follow equivalent trend with lower diversity coinciding with analyses being sequence driven. Here  
136 the relative date span is the time between the first and last sample, divided by the height of the  
137 outbreak tree and thus should be indicative of the information content of the dates. The distribution  
138 of relative date-span appears random across classifications, unlike the distribution of site patterns  
139 (Fig 3B, S3).

## 140 Empirical Results

141 We analysed data from two SARS-CoV-2 transmission clusters from 2020 in Australia to demonstrate  
142 that date-driven and sequence-driven analyses can arise in practice (table 2). The first cluster is  
143 classified as sequence-driven, with  $r_{SD} = 0.223$  indicating an appreciable difference between the  
144 sequence posterior and complete data.  $d_{SD} = 0.078$  adds that date data also drives an effect of  
145 similar size, offering the interpretation that both date and sequence data are influential in this  
146 analysis. The second cluster is classified as date-driven, but with  $r_{SD} = 0.009$  and  $d_{SD} = 0.008$ .  
147 The low  $r_{SD}$  value indicates a near-negligible difference between date, sequence, and complete data  
148 posteriors. Since  $r_{SD}$  is low,  $d_{SD}$  is necessarily also low. Due to this, classification is effectively  
149 meaningless and it can be concluded that both date and sequence data drive a highly congruent  
150 signal. Moreover,  $W_N$  for both analyses is more than double each of  $W_S$  and  $W_D$ , which affirms  
151 that both sources of data contribute to the posterior deviating from the prior and are therefore  
152 informative with respect to the prior in both analyses.

Table 2: Empirical data

	Cluster 1	Cluster 2
n	112	188
Classification	Seq-Driven	Date-Driven
$r_{SD}$	0.223	0.009
$d_{SD}$	0.078	0.008
$W_D$	0.192	0.001
$W_S$	0.114	0.009
$W_N$	0.325	0.481

## Discussion

The results of our simulation study add clarity to previous work showing that sampling times contribute substantially to phylodynamic inference under the birth death (Volz and Frost, 2014; Featherstone et al., 2021). We demonstrate that lower sequence diversity often precludes sequence data from a comparable effect. We also demonstrate that sequence data are not always secondary in influence and can drive inference of  $R_0$  in some instances, affirming the sensitivity of the birth-death to the signal encoded in sequence data. The tendency for date data to drive inference more than sequence data may be explained by the reduction in uncertainty that each data source offers. Dates impose a hard bound on topology by restricting tree space to a subset of topologies that agree with the chronology of sampling times. Conversely, sequence data inform topology through phylogenetic likelihood, but do not definitively constrain tree space in the same way as date data.

Our method offers novel insight for phylodynamics practitioners because the contribution of sequence data relative to sampling dates is often questioned in birth death analyses of densely sequenced outbreaks. It offers a reproducible approach to answering this question so the influence of genomic data can be commented on. For example, this is useful in a public health reporting context so phylodynamics experts can comment on the drivers inference as new data emerge. As such it offers a tool to initiate research into optimal sampling design for phylodynamic analysis. Any resulting theory can only be speculative at best, given the unpredictable nature of evolution, however this is an important consideration for the future as the scale of pathogen genome sequencing

172 increases.

## 173 Data Archival

174 All scripts used to simulate and analyse data are available at [https://github.com/LeoFeatherstone/](https://github.com/LeoFeatherstone/phyloDataSignal.git)  
175 [phyloDataSignal.git](https://github.com/LeoFeatherstone/phyloDataSignal.git). The Feast package, containing our date estimator, is available at [https:](https://github.com/tgvaughan/feast.git)  
176 [//github.com/tgvaughan/feast.git](https://github.com/tgvaughan/feast.git).

## 177 Supplementary Methods

### 178 Simulation Study

179 We simulated 100 outbreaks of 100 cases under a birth death process using the **Tree-Sim** R package  
180 (Stadler, 2019). The birth rate was set to 2.5, death rate 1, corresponding to  $R_0 = 2.5$ , and sampling  
181 probability  $p = 1$ , resulting in trees with 100 tips. We then extended this to a set of 200 outbreaks  
182 by sampling again with probability  $p = 0.5$ , resulting in trees of 50 tips. We used a consistent seed  
183 such that each outbreak with  $p = 0.5$  corresponds to a subsample of another with  $p = 1$ , allowing  
184 us to assess the effect of sampling proportion on inferring  $W_{\bullet}$ . For each outbreak, we simulated two  
185 sequence alignments of length 20000, which is roughly average for RNA viruses (Sanjuán et al., 2010).  
186 We set an HKY model with evolutionary rate set to either  $10^{-3}$  or  $10^{-5}$  *subs/site/time* using Seq-  
187 Gen Rambaut and Grass (1997). Our choice of evolutionary rates allows us to compare the effects  
188 higher and lower sequence information with the former corresponding to about 20 substitutions per  
189 infection, and 0.2 for the latter. The above resulted in 400 alignments to test in the four treatments  
190 described above. We analysed each under a birth-death model with a *Uniform*[0, 5] prior for  $R_0$  and  
191 all other parameters set to the true value for simplicity and to disentangle any impacts of parameter  
192 nonidentifiability (Louca et al., 2021).

## 193 Empirical Data

194 We analysed two similar SARS-CoV-2 datasets taken from (Lane et al., 2021). They consisted of 112  
195 and 188 samples respectively. We analysed each dataset under the four conditions above. In each,  
196 we placed a *Lognormal*( $mean = 1, sd = 1.25$ ) prior on  $R_0$  and an *Inv - Gamma*( $\alpha = 5.807, \beta =$   
197  $346.020$ ) prior on the becoming-uninfectious rate ( $\delta$ ) following estimates of the duration of infection  
198 ( $= \frac{1}{\delta}$ ) in Lauer et al. (2020). We also fixed the sampling proportion to  $p = 0.8$ , and placed an  
199 *Exp*( $mean = 0.019$ ) prior on the origin, corresponding to a lag of up to one week between the index  
200 case the first putative transmission event.

## 201 Validating the Wasserstein Metric

202 We use the transport R package to calculate the Wasserstein metric. We conducted an analysis  
203 to ensure that classification using the Wasserstien statistic reflects differences between date and  
204 sequence data, rather than noise alone. For each of the 400 test datasets, we subsampled each pos-  
205 terior 100 times with probability 0.5 and reclassified each subsampled dataset ( $n=40000$ ). Of these,  
206 only 329 were misclassified. Of the 400 simulated datasets, those with any degree of misclassified  
207 subsamples had substantially smaller differences between Wasserstein distance to the date-only and  
208 sequence-only posteriors ( $d_{SD}$ ) (Figure S1). Misclassification occurred for ( $d_{SD}$ ) less than roughly  
209  $10^{-1.5}$ , with complete reliability above this level. Differences below  $10^{-1.5}$  correspond to a level  
210 of difference between data and sequence only posteriors where classification is of little significance.  
211 Classification is wholly reliably above this threshold, where classification is more warranted.

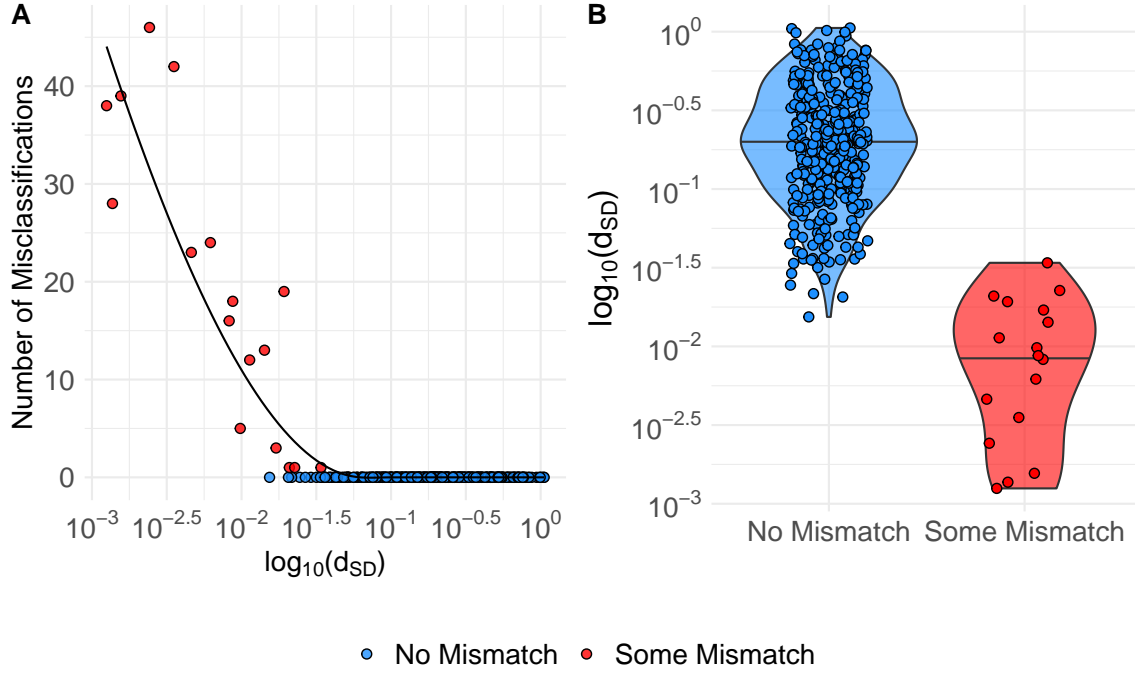


Figure S1: A) Each point presents the number of misclassification in subsampling posterior  $R_0$  for each of the 400 simulated datasets. X-axis is the log transformed difference between  $W_S$  and  $W_D$ . B) Violin plots with jittered points of the difference between  $W_S$  and  $W_D$  for simulated alignments where there was wither some one no misclassification. Both A and B support that misclassification only occurs where the difference between  $W_S$  and  $W_D$  is negligible, and classification is not meaningful in the first instance.

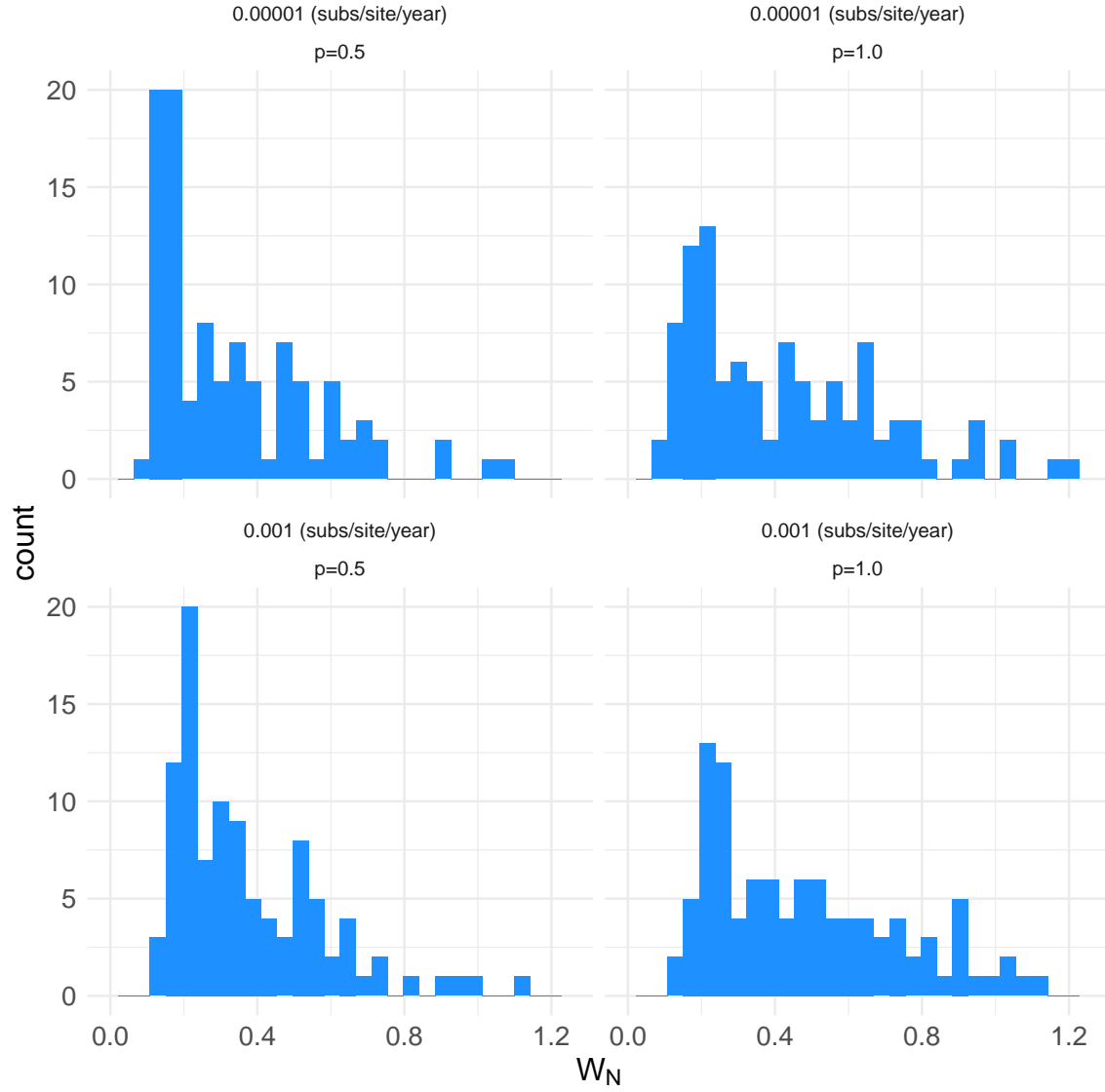


Figure S2: Histogram of  $W_N$  for each simulated dataset, separated by evolutionary rate and sampling proportion.  $W_N$  ranges from 0.1 to 1.2, such that simulated data provide additional information beyond that of the prior in each analysis.

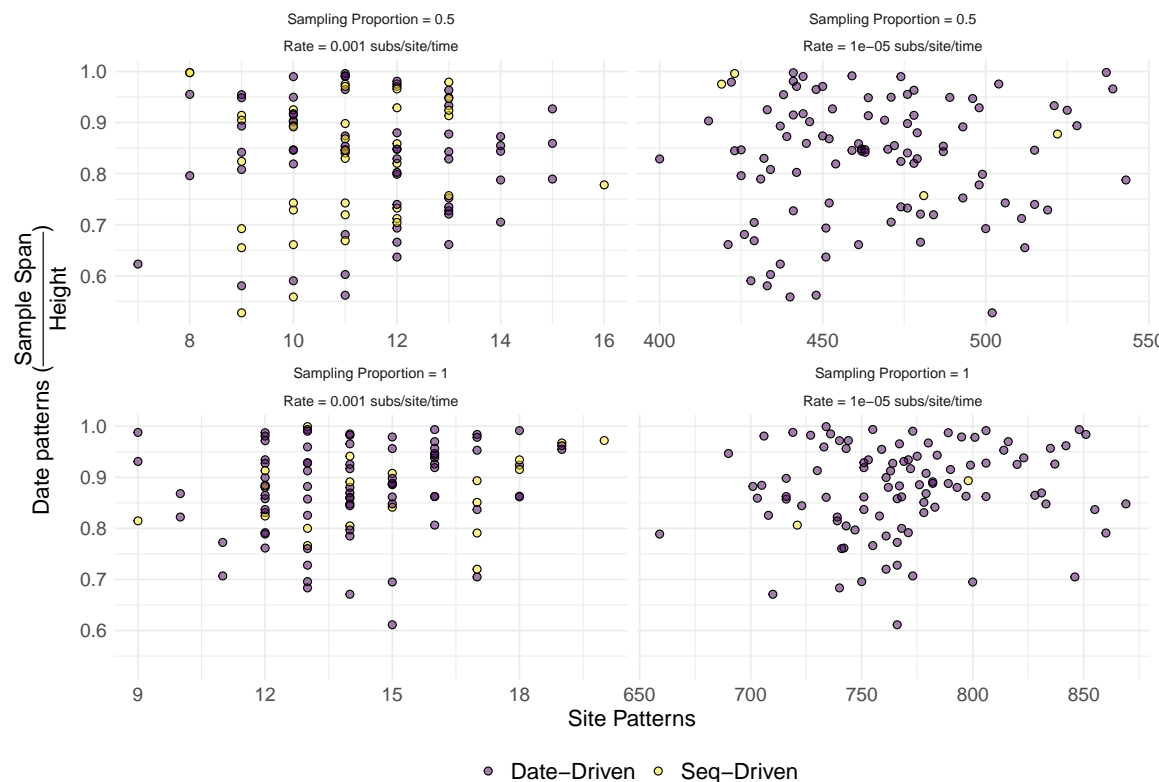


Figure S3: Date patterns ( $= \frac{\text{Sampling Span}}{\text{Height}}$ ) against site patterns for each simulated dataset. Plots are separated by evolutionary rate and sampling proportion such that there are 400 points coloured by Wasserstein Classification across the entire figure. Higher evolutionary rates increase the proportion of Sequence driven datasets, but within each rate there is no clear pattern in date patterns, site patterns, or sampling rate driving classification.

## Acknowledgements

LAF is grateful to Swissnex for awarding a Student Research Scholarship to foster this research. SD and LAF were received funding from the Australian Research Council (DE190100805), the Australian Medical Research Futures Fund (MRF9200006), and the National Health and Medical Research Council (APP1157586)

## References

G. Baele, S. Dellicour, M. A. Suchard, P. Lemey, and B. Vrancken. Recent advances in computational phylodynamics. *Current opinion in virology*, 31:24–32, 2018.



220 V. Boskova, T. Stadler, and C. Magnus. The influence of phylodynamic model specifications on  
 221 parameter estimates of the zika virus epidemic. *Virus evolution*, 4(1):vex044, 2018.

222 R. Bouckaert, T. G. Vaughan, J. Barido-Sottani, S. Duchêne, M. Fourment, A. Gavryushkina,  
 223 J. Heled, G. Jones, D. Kühnert, N. D. Maio, M. Matschiner, F. K. Mendes, N. F. Müller, H. A.  
 224 Ogilvie, L. d. Plessis, A. Poppinga, A. Rambaut, D. Rasmussen, I. Siveroni, M. A. Suchard, C.-H.  
 225 Wu, D. Xie, C. Zhang, T. Stadler, and A. J. Drummond. BEAST 2.5: An advanced software  
 226 platform for Bayesian evolutionary analysis. *PLOS Computational Biology*, 15(4):e1006650, Apr.  
 227 2019. ISSN 1553-7358. doi: 10.1371/journal.pcbi.1006650. URL [https://journals.plos.org/](https://journals.plos.org/ploscompbiol/article?id=10.1371/journal.pcbi.1006650)  
 228 [ploscompbiol/article?id=10.1371/journal.pcbi.1006650](https://journals.plos.org/ploscompbiol/article?id=10.1371/journal.pcbi.1006650). Publisher: Public Library of Sci-  
 229 ence.

230 L. du Plessis and T. Stadler. Getting to the root of epidemic spread with phylodynamic analysis of  
 231 genomic data. *Trends in Microbiology*, 23(7):383–386, 2015.

232 L. A. Featherstone, F. Di Giallonardo, E. C. Holmes, T. G. Vaughan, and S. Duchêne. Infec-  
 233 tious disease phylodynamics with occurrence data. *Methods in Ecology and Evolution*, 12(8):  
 234 1498–1507, 2021. doi: <https://doi.org/10.1111/2041-210X.13620>. URL [https://besjournals.](https://besjournals.onlinelibrary.wiley.com/doi/abs/10.1111/2041-210X.13620)  
 235 [onlinelibrary.wiley.com/doi/abs/10.1111/2041-210X.13620](https://besjournals.onlinelibrary.wiley.com/doi/abs/10.1111/2041-210X.13620).

236 C. R. Lane, N. L. Sherry, A. F. Porter, S. Duchene, K. Horan, P. Andersson, M. Wilmot, A. Turner,  
 237 S. Dougall, S. A. Johnson, et al. Genomics-informed responses in the elimination of covid-19 in  
 238 victoria, australia: an observational, genomic epidemiological study. *The Lancet Public Health*, 6  
 239 (8):e547–e556, 2021.

240 S. A. Lauer, K. H. Grantz, Q. Bi, F. K. Jones, Q. Zheng, H. R. Meredith, A. S. Azman, A. S. Azman,  
 241 N. G. Reich, and J. Lessler. The incubation period of coronavirus disease 2019 (covid-19) from  
 242 publicly reported confirmed cases: Estimation and application. *Annals of Internal Medicine*, 172  
 243 (9):577–582, 2020. doi: 10.7326/M20-0504. URL <https://doi.org/10.7326/M20-0504>. PMID:  
 244 32150748.

245 S. Louca, A. McLaughlin, A. MacPherson, J. B. Joy, and M. W. Pennell. Fundamental identifiability  
 246 limits in molecular epidemiology. *Molecular Biology and Evolution*, 38(9):4010–4024, 2021.

247 A. Rambaut and N. C. Grass. Seq-Gen: an application for the Monte Carlo simulation of DNA  
 248 sequence evolution along phylogenetic trees. *Bioinformatics*, 13(3):235–238, 1997. ISSN 1367-  
 249 4803, 1460-2059. doi: 10.1093/bioinformatics/13.3.235. URL [https://academic.oup.com/](https://academic.oup.com/bioinformatics/article-lookup/doi/10.1093/bioinformatics/13.3.235)  
 250 [bioinformatics/article-lookup/doi/10.1093/bioinformatics/13.3.235](https://academic.oup.com/bioinformatics/article-lookup/doi/10.1093/bioinformatics/13.3.235).

251 R. Sanjuán, M. R. Nebot, N. Chirico, L. M. Mansky, and R. Belshaw. Viral mutation rates. *Journal*  
 252 *of virology*, 84(19):9733–9748, 2010.

253 T. Stadler. Sampling-through-time in birth–death trees. *Journal of Theoretical Biology*, 267(3):  
 254 396–404, Dec. 2010. ISSN 00225193. doi: 10.1016/j.jtbi.2010.09.010. URL [https://linkinghub.](https://linkinghub.elsevier.com/retrieve/pii/S0022519310004765)  
 255 [elsevier.com/retrieve/pii/S0022519310004765](https://linkinghub.elsevier.com/retrieve/pii/S0022519310004765).

256 T. Stadler. *TreeSim: Simulating Phylogenetic Trees*, 2019. URL [https://CRAN.R-project.org/](https://CRAN.R-project.org/package=TreeSim)  
 257 [package=TreeSim](https://CRAN.R-project.org/package=TreeSim). R package version 2.4.

258 T. Stadler, R. Kouyos, V. von Wyl, S. Yerly, J. Böni, P. Bürgisser, T. Klimkait, B. Joos, P. Rieder,  
 259 D. Xie, et al. Estimating the basic reproductive number from viral sequence data. *Molecular*  
 260 *biology and evolution*, 29(1):347–357, 2012.

261 E. M. Volz and S. D. W. Frost. Sampling through time and phylodynamic inference with coales-  
 262 cent and birth–death models. *Journal of the Royal Society Interface*, 11(101), Dec. 2014. ISSN  
 263 1742-5689. doi: 10.1098/rsif.2014.0945. URL [https://www.ncbi.nlm.nih.gov/pmc/articles/](https://www.ncbi.nlm.nih.gov/pmc/articles/PMC4223917/)  
 264 [PMC4223917/](https://www.ncbi.nlm.nih.gov/pmc/articles/PMC4223917/).

265 E. M. Volz, K. Koelle, and T. Bedford. Viral phylodynamics. *PLoS computational biology*, 9(3):  
 266 e1002947, 2013.